ACS Biomaterials SCIENCE & ENGINEERING

pubs.acs.org/journal/abseba

Letter

Reduction of Infectivity of SARS-CoV-2 by Zinc Oxide Coatings

Mohsen Hosseini,[†] Saeed Behzadinasab,[†] Alex W.H. Chin,[†] Leo L.M. Poon,* and William A. Ducker*

Cite This: *ACS Biomater. Sci. Eng.* 2021, 7, 5022−5027

Read Online

ACCESS | Metrics & More | Article Recommendations | Supporting Information

ABSTRACT: We developed antimicrobial coatings from ZnO particles that reduce the infectivity of SARS-CoV-2 suspensions by >99.9% in 1 h. The advantage of a coating is that it can be applied to a variety of objects, e.g., hand rails and door knobs, to hinder the spread of disease. Two porous coatings were prepared: one from submicrometer zinc oxide particles bound with silica menisci and the other from zinc oxide tetrapods bound with polyurethane. Experiments on glass coatings show that infectivity depends on porosity for hydrophilic materials, wherein aqueous droplets are imbibed into the pores.

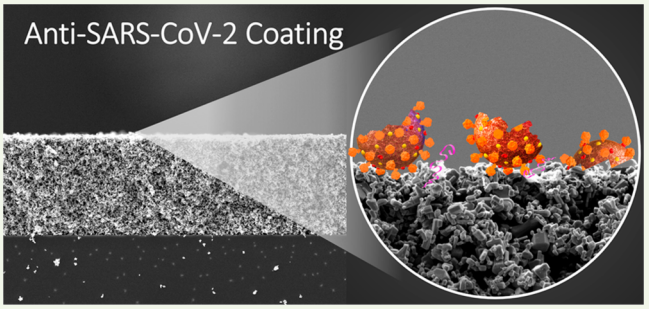

KEYWORDS: *SARS-CoV-2, zinc oxide, zinc oxide tetrapod, coating, coronavirus, antiviral, COVID-19*

Downloaded via VIRGINIA POLYTECH INST STATE UNIV on June 8, 2022 at 19:04:25 (UTC).
See https://pubs.acs.org/sharingguidelines for options on how to legitimately share published articles.

1. INTRODUCTION

Coronavirus disease 2019 (COVID-19) created many negative economic, health, and psychological impacts on human life. During the period January 2020 to May 2021, more than 150 million positive COVID-19 cases were reported worldwide and more than 3.5 million people died as a result of the disease.[1] The causative virus, severe acute respiratory syndrome coronavirus-2, abbreviated as SARS-CoV-2, is believed to be transmitted through two routes. The primary mode of the transmission is through the inhalation of respiratory droplets generated by infected people as a result of breathing, speaking, coughing, sneezing, etc.[2] Small droplets remain suspended in air for up to 30 h,[3] and a healthy individual can become infected simply by inhaling them. Another route of SARS-CoV-2 transfer is through fomites.[4,5] Larger respiratory droplets can land on objects and infected people may transfer contaminated liquid directly to objects by touching their face and then an inanimate object. Such solids contaminated with virus are known as fomites. Examples of fomites are everyday objects such as door handles, railings, elevator buttons, and check-out facilities contaminated by respiratory droplets or dried residue of viable virus. SARS-CoV-2 can remain viable up to 7 days on nonporous solid surfaces,[6,7] so there is a significant window of opportunity for infection via this route.

An animal study showed that although inhalation of contaminated droplets is the main route of infection, fomite transmission also occurred,[4] and a modeling study showed fomite transmission was responsible for 25% of infections.[8] The mechanism for human infection is simple: SARS-CoV-2 can be transferred by touching a contaminated solid, and then when the hand touches the nose, mouth or eyes, the virus may enter the mucus and find its way to the epithelial cells.[9,10] Recent unpublished work has shown that the virus can transfer from a contaminated surface to skin.[5]

A significant difficulty with the decontamination of solids is that most disinfectants kill only microbes that were present before the disinfectants were used. Almost immediately after the surface is treated with disinfectant, an infected person can again contaminate the solid.[11] Effective control by this method therefore requires very frequent disinfection, which is labor intensive, expensive, and may cause loss of productivity. For example, a train or bus may need to be temporarily out of service during disinfection.

An alternative approach is to use coatings that are designed to provide an ongoing reduction of infectivity. That means they inactivate or kill microbes long after the coating is applied. Copper-based coatings have already been reported to inactivate SARS-CoV-2.[12−15] The virus has also been reported to be less stable on nanostructured aluminum surfaces[16] and light-activated titanium dioxide.[17] Here, we use zinc oxide as an alternative ingredient that has the ability to inactivate SARS-CoV-2. ZnO has a different color (white) compared to copper compounds and has different stability and toxicity. Zn^{2+} and ZnO nanoparticles have recently been shown to have activity against SARS-CoV-2.[18,19]

Zinc oxide (ZnO) particles have been shown to be antibacterial[20,21] and antiviral.[22,23] Prior coatings of ZnO particles on surfaces focused on simply depositing the particles

Received: August 22, 2021
Accepted: September 23, 2021
Published: October 6, 2021

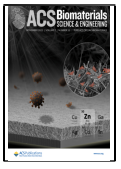

© 2021 American Chemical Society

on a surface using ultrasonic irradiation,[24] flame spray pyrolysis,[25] or thin film coater machine.[26] Without immobilized particles, this approach may not have a long-lasting effect. Several ZnO nanocomposites have previously been developed and tested against bacteria and have been found to kill *Escherichia coli*.[27,28]

Here, we describe ZnO coatings that were designed such that the coating adhered to the solid without encapsulating the particles within an adhesive. If the active ingredient is a small ion or molecule that elutes from the coating, then the coating should at least be permeable to that ion or small molecule or to the microbe. Coatings can obviously not achieve "contact killing" (where the microbe is inactivated or killed by physical contact) if the solid particle is encapsulated in an impermeable matrix.

Two coatings are described, the first of which consists of crystalline 300 nm ZnO particles that are held together by solid glass menisci produced by a modified version of the Stöber process using tetraethyl orthosilicate (TEOS).[29,30] The menisci form adhesive junctions between the particles but the menisci are sufficiently small that there remains a large exposed surface area of ZnO for inactivation of microbes. First, the liquid menisci were created, and then the menisci were solidified using a gas phase catalyst. The solids loading was 38 g/m^2. The second coating was fabricated from crystalline ZnO with a tetrapodal morphology (ZnO-T). Because the legs avoid close packing, ZnO-T is a low density material with large pores.[31] In this work, we adhered the ZnO tetrapod particles with polyurethane (PU), similarly to prior work with Cu_2O,[12] but with much less PU. Less PU produces a more hydrophilic coating, thereby allowing imbibition of the droplet. The solids loading was 56 g/m^2. We refer to the coatings as ZnO/Silica and ZnO-T/PU coatings. Our results show that both coatings were very successful at reducing infection by SARS-CoV-2.

In addition, the porosity of an antiviral coating is important for several reasons: it may affect the drying time,[13,32] the surface area of active material, the transport time, and perhaps the ability to recover virus that may become adsorbed or otherwise trapped in the porosity.[10] We directly investigate the trapping/adsorption hypothesis by comparing a porous glass coating to a nonporous glass surface.

2. RESULTS

2.1. Characterization. The active part of the coating is where contact occurs between the droplet of virus suspension and the solid. Therefore, the wetting and imbibition are critical aspects of coating performance. The zinc oxide particles are intrinsically hydrophilic; they immediately fall through the air−water interface. The contact angle of water droplet on ZnO/Silica was 72° ± 3° (droplet size = 5 μL, error shows 95% confidence interval from 5 independent measurements, see Figure S1), and the droplet partially and slowly imbibes into the coating (Figure S2). The advancing water contact angle of ZnO-T/PU was 13° ± 23° (1 day after plasma treatment; droplet size ≈ 10 μL). For the ZnO-T/PU sample, the error reflects that angles were as high as 40°. For the low contact angles, the droplet was immediately imbibed into ZnO-T/PU coating (Figure S3). In contrast to the earlier coatings fabricated from Cu_2O and PU where the contact angle increased with time, the contact angle of ZnO-T/PU was only 17° ± 22° after 11 days. The lack of "recovery" of the angle is probably because there is very little PU on the surface. The maintenance of wettability is important for achieving contact between the active ingredient and virus in a droplet.

The microstructure of the coatings is shown in scanning electron microscope (SEM) images (Figure 1). The shapes of individual particles are visible, which demonstrate the that they were not engulfed in silica or PU, and the porosity is also evident. Figure 1E, F shows the cross-sectional images that enable measurement of the thicknesses of the ZnO/Silica and ZnO-T/PU, which were 30 ± 2 μm and 220 ± 50 μm, respectively (thickness ±95% confidence interval). The cross sections also demonstrate that the porosity is throughout the coatings and shows a uniform thickness. High-magnification images of the ZnO/Silica (Figure 1G) indicate necks between the particles that were created by the Stöber process.

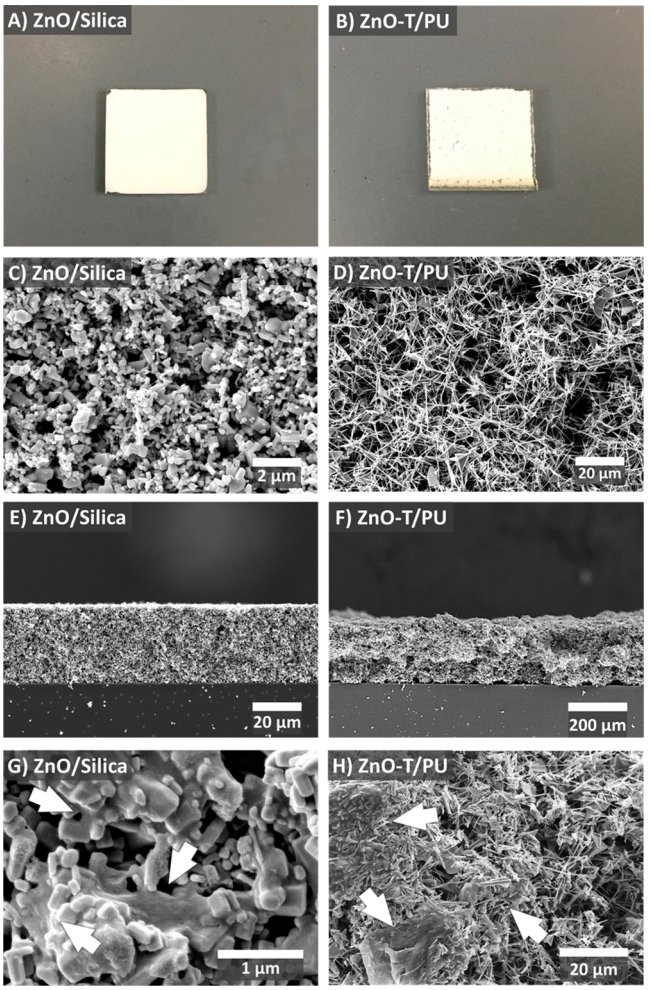

Figure 1. Photograph of (A) ZnO/Silica coating and (B) ZnO-T/PU coating. Each sample is 12 mm × 12 mm × 1 mm. SEM images of (C) surface ZnO/Silica, (D) surface ZnO-T/PU, (E) cross-section of ZnO/Silica coating, (F) cross-section of ZnO-T/PU coating, (G) silica menisci (necks) between ZnO particles in ZnO/Silica coating, and (H) higher-resolution cross-sectional image of the ZnO-T/PU sample. Arrows point to regions where the coating is amorphous and therefore there is a large volume fraction of PU. Other regions have a lower volume fraction of PU and hence greater porosity. Note scale difference for ZnO/Silica compared to ZnO-T/PU SEM images.

The outer few nanometers of each coating was selectively probed by X-ray photoelectron spectroscopy (XPS). The XPS spectrum of the ZnO/Silica coating (Figure S4) shows that

https://doi.org/10.1021/acsbiomaterials.1c01076
ACS Biomater. Sci. Eng. 2021, 7, 5022−5027

36% of the surface is Zn, which given the stoichiometry of ZnO is consistent with 73% of the surface being ZnO. There is negligible silicon, which shows that the silica produced by the Stöber process does not cover the ZnO particles but is confined to menisci, as planned. This was confirmed by the energy-dispersive X-ray spectroscopy (EDS) analysis of the top micrometer of the coating that showed a zinc to oxygen ratio of 0.99 ± 0.04:1, again consistent with only a small amount of silica (SiO_2) in the coating. The silica menisci were too small to resolve their chemistry by EDS imaging. The zinc oxide tetrapod is known to pack with a low mass to volume ratio because the tetrapod has arms that inhibit packing,[31] and the very high void fraction is clearly shown in Figure 1: the tetrapods in the coating are not engulfed in PU. XPS reveals that the ZnO-T/PU coating has twice the fraction of carbon (20%) as the ZnO/Silica, which is consistent with the presence of PU in the coating. We also measured the composition of the surface with EDS, and the ratio of zinc to oxygen was 1.1:1.0, which is consistent with the stoichiometric value of 1:1.

X-ray diffraction (XRD, Figure S5) showed that both coatings were predominantly crystalline ZnO with the wurtzite structure.

2.2. ZnO Coatings Reduce Infectivity of SARS-CoV-2. We tested the reduction of SARS-CoV-2 suspensions after 5 μL droplets were placed on ZnO/Silica or ZnO-T/PU coatings. The droplet remained on each coating for a predefined period of time, and then the virus was eluted from the solid, and then the eluant was used to infect VERO E6 cells using a $TCID_{50}$ assay (see the methods in the Supporting Information). SARS-CoV-2 spontaneously loses its ability to infect cells over time, so in each case, we compare the outcome on the coating to the outcome on an uncoated surface. The coating is on glass, so the uncoated sample is plain glass. We use the word *Reduction* to compare the results on the coating to results on the uncoated glass at the same time point:

$$\text{log reduction} = \text{mean}[\log_{10}(\text{glass control titer})] - \text{mean}[\log_{10}(\text{sample titer})] \quad (1)$$

$$\%\text{reduction} = (1 - 10^{-\text{log reduction}})100\% \quad (2)$$

Both ZnO coatings caused a dramatic decrease in the infectivity (Figure 2): the infectivity of the SARS-CoV-2 dropped by 99.99% in 1 h (i.e., more than 4 logs), whereas only a 0.7 log drop in infectivity was observed on the uncoated glass within the same period of time. The central idea of this work is that a coating can decrease the activity of SARS-CoV-2 on a coated solid more rapidly than on the uncoated solid, so we compared the results on each ZnO coating to results on the uncoated glass. The ZnO/Silica coating caused a > 99.98% *Reduction* (>3 log reduction) and ZnO-T/PU caused a 99.97% *Reduction* in 1 h. The reason for the "greater than symbol" is that all the ZnO/Silica titers were below the lower limit of detection. For the ZnO-T/PU coating, two of three measurements were below the detection limit, and the average was calculated as if these measurements were at the detection limit. The one-tailed 95% confidence intervals demonstrate more than 99.92% and more than 99.89% SARS-CoV-2 titer *Reduction* after 1 h on ZnO/Silica and ZnO-T/PU coatings, respectively.

We tested the adhesion of our coatings according to the ASTM D3359 standard. Figure S8 shows that both coatings demonstrated a satisfactory adhesion, where the adhesion for

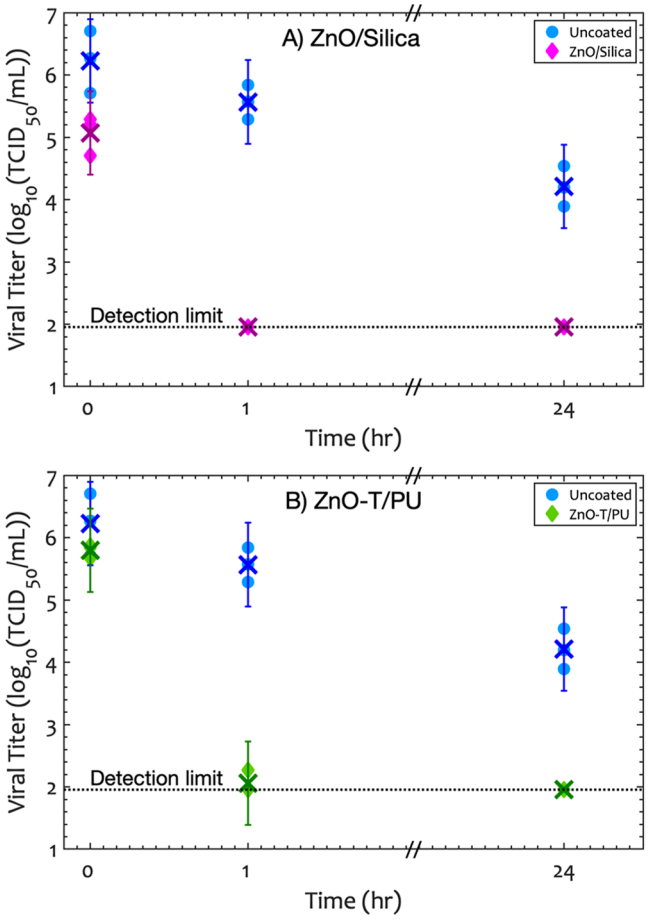

Figure 2. Decay of SARS-CoV-2 $TCID_{50}$ titer on (A) ZnO/Silica and (B) ZnO-T/PU coatings on glass. Diamonds and circles show independent titer measurements, × represents the average of the log titer at each time, and the dashed line shows the detection limit of the assay (90 $TCID_{50}$/mL). Error bars are the 95% confidence interval. In comparison to uncoated glass, the virus titer has a 99.98% *Reduction* on ZnO/Silica ($p = 1 \times 10^{-3}$, one tail, unpaired) and 99.97% *Reduction* on ZnO-T/PU after 1 h ($p = 7 \times 10^{-5}$, one tail, unpaired).

ZnO/Silica and ZnO-T/PU were rated at least 3B and 3A, respectively.

2.3. Discussion. We used zinc oxide particles as the active antipathogenic ingredient of our coatings. A key advantage of ZnO is the low level of toxicity to humans. The United States Food and Drug Administration (FDA) has designated ZnO as "generally recognized as safe" (GRAS).[33]

SARS-CoV-2 is a novel pathogen, so the mechanism of action of ZnO particularly against SARS-CoV-2 is unknown, but here we describe the mechanisms against other organisms, which we consider to be likely mechanisms against SARS-CoV-2. Zinc oxide is known to demonstrate its antipathogenic properties through two main mechanisms:[34−37] by Zn^{2+} ion release and by creation of reactive oxygen species (ROS). ZnO particles release Zn^{2+} ions in aqueous solutions. These ions would mediate the attachment of negatively charged cell membrane to zinc oxide particles, causing a localized increase in Zn^{2+} ion concentration that eventually leads to membrane leakage and cell death accordingly.[38,39] It has been reported that $OH^{\bullet}$, $O_2^{\bullet}$, and H_2O_2 are generated on the ZnO surface.[37] H_2O_2 is an active agent and when it enters cells, it exerts oxidative stress that leads to damage or killing of bacteria.[40] It has also been reported that the trapped oxygen within the

https://doi.org/10.1021/acsbiomaterials.1c01076
ACS Biomater. Sci. Eng. 2021, 7, 5022−5027

porosity of ZnO particles further reinforces the generation of ROS.[40] It is possible that the action against a virus might be different. Despite the potent antimicrobial activity, ZnO has a very low level of cytotoxicity on L929 cells,[41] making it highly biocompatible for use in a variety of applications.[42]

As described in the introduction, the use of porous coatings is a substantial advantage because the porosity may affect the drying time, the surface area of active material, the transport time, and the ability to recover virus that may become adsorbed or otherwise trapped in the porosity.[10] To date, there has been no direct check of whether porosity affects the infectivity because there are no results in the literature that compare porous and nonporous surfaces of the same material. To understand how infectivity is lost because of porosity, we have compared titers obtained from glass and porous glass that have very similar chemistry (see Figure S9 for XPS results), so the effect of chemistry is removed from the comparison. Glass has no active material and the decay of SARS-CoV-2 on glass is very slow, so there is no effect of changing the amount of active material or transport to or of the active material.[7,43] The comparison thus directly tests the effect of porosity.

Figure 3 compares the infectivity of SARS-CoV-2 recovered from droplets on porous and nonporous glass. It is

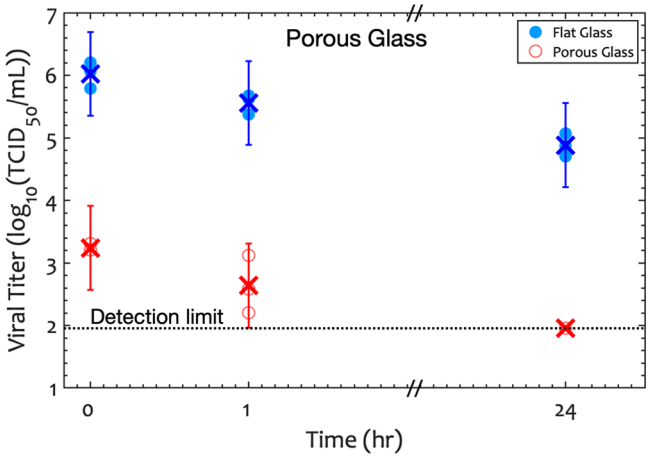

Figure 3. Decay of SARS-CoV-2 $TCID_{50}$ titer on porous glass compared to flat glass. The two glass surfaces are soda-lime glass, and have similar chemistry (see XPS in the Figure S9). Diamonds and circles show independent titer measurements, × represents the average of the log titer at each time, the dashed line shows the detection limit of the assay (90 $TCID_{50}$/mL), and error bars are the 95% confidence interval. The virus titers on porous glass at 0 and 1 h time points are not statistically different ($p = 0.33$, one tail, unpaired), confirming its inactive nature against SARS-CoV-2.

immediately apparent that the infectivity is much lower from the porous glass, so we have shown unambiguously that the introduction of porosity reduces infectivity as measured by elution and $TCID_{50}$ measurements.

Results at time zero are instructive. Aqueous droplets are immediately imbibed into the porous hydrophilic glass: imbibition occurs before elution, which in practice is <1 min after the droplet is placed on the solid. Therefore, the "zero" time point assays recovery from within the porosity. The majority of the infectivity is lost immediately on the porous glass, with the porous glass titer 2.9 logs below that of the nonporous glass. This compares sharply with the ZnO results, where the viral titers were much greater at time zero. For ZnO-T/PU, the imbibition also occurs before elution so time zero titer also assays liquid from the porosity, but in this case the *Reduction* is only 0.4 logs. In summary, the vast majority of infectivity on the porous glass is lost immediately in the porosity but little is lost in the porous ZnO-T/PU. The ZnO/Silica has a much higher contact angle (72° ± 3°), which prevents immediate imbibition. Student's t tests showed that the viral titer at 0 h on porous glass is significantly smaller than that on ZnO/Silica ($p = 6 \times 10^{-3}$) and ZnO-T/PU ($p = 3 \times 10^{-5}$) coatings.

It is also instructive to compare the 1 and 0 h time points for the same material using the following equation:

$$\log 1\text{ h reduction} = \text{mean}[\log_{10}(0\text{ h titer})] - \text{mean}[\log_{10}(1\text{ h titer})] \quad (3)$$

The log 1 h reduction on glass is 0.4 and that on porous glass is 0.6; these values are not significantly different ($p = 0.33$). So, the glass is an inactive material because even by increasing the porosity to make more surface area and a faster transport time, there is no additional loss of infectivity over time. The main effect of porosity is simply to reduce recovery. The porosity could also affect drying time,[13] which has been hypothesized as a parameter for inactivation.[44]

For the ZnO materials, by comparison, there is significant loss of infectivity ($p < 4 \times 10^{-3}$) over time. The log 1 h reduction is at least 3.1 on ZnO/Silica and at least 3.7 on ZnO-T/PU. This is consistent with an active material. So, in summary, the ZnO coatings reduce infectivity in two ways: (1) some of the virus becomes trapped in the porosity and (2) once the droplet goes into the pores or dries onto the surface, there is an ongoing loss of infectivity that we attribute to the antimicrobial properties of ZnO. The active antimicrobial activity of ZnO is superior to an inactive porous material because the active material has the potential to kill bacteria that may linger in the porosity.

Recent work has also shown activity of Zn products against SARS-CoV-2. Gopal et al.[19] demonstrated a reduction of SARS-CoV-2 of about 90% by coating fibers with Zn^{2+} ions and El-Megharbel et al.[18] showed that a ZnO particle spray disinfectant caused a 40% reduction. These results are consistent with our results but show lower reductions. In contrast, Merkl et al.[25] did not measure activity for ZnO particles deposited on a surface.

CONCLUSIONS

In summary, we have introduced two new porous anti-SARS-CoV-2 coatings. One method used a variant of the Stöber sol–gel method to create a coating from submicrometer-sized zinc oxide particles, whereas the other method used polyurethane to immobilize zinc oxide tetrapod particles. They each reduce infectivity of the virus within 1 h: the viral titer of SARS-CoV-2 was decreased by 4 logs (>99.99%), which is a *Reduction* of at least 99.9% compared to uncoated glass. These coatings can be applied to everyday objects and therefore have the potential to reduce infection from solids and limit the spread of COVID-19 disease.

The time course of inactivation on the ZnO coatings is consistent with two actions that reduce infectivity. First, when the viral suspension droplet is imbibed into a hydrophilic porous solid, there is an immediate loss of infectivity due to the inability to recover virus from within the porous material or

https://doi.org/10.1021/acsbiomaterials.1c01076
ACS Biomater. Sci. Eng. 2021, 7, 5022−5027

from the surface of the porous material. Second, over time there is a large (>3 logs) loss of infectivity, which is consistent with an active material. For glass, by contrast, there is only a small loss of infectivity over time, which is insignificant over the first hour. The comparison of results on porous glass and nonporous glass shows definitively that loss of infectivity can occur as a result of imbibition into a porous hydrophilic material.

■ ASSOCIATED CONTENT

Supporting Information

The Supporting Information is available free of charge at https://pubs.acs.org/doi/10.1021/acsbiomaterials.1c01076.

Materials and methods, time lapse of imbibition of a droplet in ZnO/TEOS film (Figure S1), disc pattern imbibition of a droplet in ZnO/TEOS film (Figure S2), advancing contact angles measurement of ZnO-T/PU coating (Figure S3), XPS spectra and the elemental analysis of the outer surface of the coatings (Figure S4), XRD pattern of the coatings (Figure S5), effect of a 3 min Argon plasma cleaning in the preparation of ZnO-T/PU coating (Figure S6), size distribution histogram of submicrometer ZnO particles (Figure S7), ASTM D3359 adhesion test result for ZnO coatings (Figure S8), table of XPS results for glass and SEM image of porous glass surface (Figure S9), decay of SARS-CoV-2 $TCID_{50}$ titer on silica and polyurethane coatings and its comparison to glass (Figure S10), $TCID_{50}$ assay data for Figure 2 (Table S1), and $TCID_{50}$ assay data for Figure 3 (Table S2) (PDF)

■ AUTHOR INFORMATION

Corresponding Authors

Leo L.M. Poon − *School of Public Health, LKS Faculty of Medicine, The University of Hong Kong, Hong Kong, China; Centre for Immunity and Infection, Hong Kong Science Park, Hong Kong, China; HKU-Pasteur Research Pole, LKS Faculty of Medicine, The University of Hong Kong, Hong Kong, China*; Email: llmpoon@hku.hk

William A. Ducker − *Department of Chemical Engineering and Center for Soft Matter and Biological Physics, Virginia Tech, Blacksburg, Virginia 24061, United States;* orcid.org/0000-0002-8207-768X; Email: wducker@vt.edu

Authors

Mohsen Hosseini − *Department of Chemical Engineering and Center for Soft Matter and Biological Physics, Virginia Tech, Blacksburg, Virginia 24061, United States*

Saeed Behzadinasab − *Department of Chemical Engineering and Center for Soft Matter and Biological Physics, Virginia Tech, Blacksburg, Virginia 24061, United States;* orcid.org/0000-0002-6271-2623

Alex W.H. Chin − *School of Public Health, LKS Faculty of Medicine, The University of Hong Kong, Hong Kong, China; Centre for Immunity and Infection, Hong Kong Science Park, Hong Kong, China;* orcid.org/0000-0002-6556-9092

Complete contact information is available at: https://pubs.acs.org/10.1021/acsbiomaterials.1c01076

Author Contributions

†M.H., S.B., and A.W.H.C. contributed equally to this work

Notes

The authors declare the following competing financial interest(s): W.D. declares part ownership in a startup company that intends to produce surface coatings. The other authors declare no conflict of interest.

■ ACKNOWLEDGMENTS

The authors acknowledge use of the microscopy facilities and the X-ray diffraction machine within the NCFL and MCL at Virginia Tech. We also thank Xu Feng for capturing the XPS spectra and acknowledge use of the Surface Analysis Laboratory in the Department of Chemistry at Virginia Tech, which is supported by the National Science Foundation under Grant CHE-1531834. The authors also thank Dr. Thomas Staley for milling the glass beads used in this study. This work was supported by the National Science Foundation under Grant CBET-1902364, the Health and Medical Research Fund (COVID190116), and the National Institute of Allergy and Infectious Diseases (contract HHSN272201400006C).

■ REFERENCES

(1) *COVID-19 Dashboard by the Center for Systems Science and Engineering (CSSE) at Johns Hopkins University (JHU)*. Johns Hopkins University.https://coronavirus.jhu.edu/map.html (accessed 2021-04-25).

(2) Prather, K. A.; Wang, C. C.; Schooley, R. T. Reducing Transmission of SARS-CoV-2. *Science* **2020**, *368* (6498), 1422−1424.

(3) Duguid, J. The size and the duration of air-carriage of respiratory droplets and droplet-nuclei. *Epidemiol. Infect.* **1946**, *44* (6), 471−479.

(4) Sia, S. F.; Yan, L.-M.; Chin, A. W.; Fung, K.; Choy, K.-T.; Wong, A. Y.; Kaewpreedee, P.; Perera, R. A.; Poon, L. L.; Nicholls, J. M.; et al. Pathogenesis and transmission of SARS-CoV-2 in golden hamsters. *Nature* **2020**, *583* (7818), 834−838.

(5) Behzadinasab, S.; Chin, A. W. H.; Hosseini, M.; Poon, L. L. M.; Ducker, W. A. SARS-CoV-2 virus transfers to skin through contact with contaminated solids. *medRxiv* 2021, 2021.04.24.21256044.

(6) Van Doremalen, N.; Bushmaker, T.; Morris, D. H.; Holbrook, M. G.; Gamble, A.; Williamson, B. N.; Tamin, A.; Harcourt, J. L.; Thornburg, N. J.; Gerber, S. I.; et al. Aerosol and surface stability of SARS-CoV-2 as compared with SARS-CoV-1. *N. Engl. J. Med.* **2020**, *382* (16), 1564−1567.

(7) Chin, A. W. H.; Chu, J. T. S.; Perera, M. R. A.; Hui, K. P. Y.; Yen, H.-L.; Chan, M. C. W.; Peiris, M.; Poon, L. L. M. Stability of SARS-CoV-2 in different environmental conditions. *Lancet Microbe* **2020**, *1* (1), No. e10.

(8) Meiksin, A. Dynamics of COVID-19 transmission including indirect transmission mechanisms: a mathematical analysis. *Epidemiol. Infect.* **2020**, *148*, No. e257.

(9) *Clinical Questions about COVID-19: Questions and Answers*. Centers for Disease Control and Prevention (CDC). https://www.cdc.gov/coronavirus/2019-ncov/hcp/faq.html (accessed 2020-05-26).

(10) Hosseini, M.; Behzadinasab, S.; Benmamoun, Z.; Ducker, W. A. The Viability of SARS-CoV-2 on Solid Surfaces. *Curr. Opin. Colloid Interface Sci.* **2021**, *55*, 101481.

(11) Bhalla, A.; Pultz, N. J.; Gries, D. M.; Ray, A. J.; Eckstein, E. C.; Aron, D. C.; Donskey, C. J. Acquisition of Nosocomial Pathogens on Hands After Contact with Environmental Surfaces Near Hospitalized Patients. *Infect. Control Hosp. Epidemiol.* **2004**, *25* (2), 164−167.

(12) Behzadinasab, S.; Chin, A.; Hosseini, M.; Poon, L.; Ducker, W. A. A surface coating that rapidly inactivates SARS-CoV-2. *ACS Appl. Mater. Interfaces* **2020**, *12* (31), 34723−34727.

(13) Hosseini, M.; Chin, A. W.; Behzadinasab, S.; Poon, L. L.; Ducker, W. A. Cupric oxide coating that rapidly reduces infection by SARS-CoV-2 via solids. *ACS Appl. Mater. Interfaces* **2021**, *13* (5), 5919−5928.

(14) Hutasoit, N.; Kennedy, B.; Hamilton, S.; Luttick, A.; Rahman Rashid, R. A.; Palanisamy, S. SARS-CoV-2 (COVID-19) Inactivation Capability of Copper-Coated Touch Surface Fabricated by Cold-Spray Technology. *Manuf. Lett.* **2020**, *25*, 93−97.
(15) Hewawaduge, C.; Senevirathne, A.; Jawalagatti, V.; Kim, J. W.; Lee, J. H. Copper-impregnated three-layer mask efficiently inactivates SARS-CoV2. *Environ. Res.* **2021**, *196*, 110947.
(16) Hasan, J.; Pyke, A.; Nair, N.; Yarlagadda, T.; Will, G.; Spann, K.; Yarlagadda, P. K. Antiviral nanostructured surfaces reduce the viability of SARS-CoV-2. *ACS Biomater. Sci. Eng.* **2020**, *6* (9), 4858−4861.
(17) Micochova, P.; Chadha, A.; Hesseloj, T.; Fraternali, F.; Ramsden, J. J.; Gupta, R. K. Rapid inactivation of SARS-CoV-2 by titanium dioxide surface coating. *Wellcome Open Res.* **2021**, *6* (56), 56.
(18) El-Megharbel, S. M.; Alsawat, M.; Al-Salmi, F. A.; Hamza, R. Z. Utilizing of (Zinc Oxide Nano-Spray) for Disinfection against "SARS-CoV-2" and Testing Its Biological Effectiveness on Some Biochemical Parameters during (COVID-19 Pandemic)—" ZnO Nanoparticles Have Antiviral Activity against (SARS-CoV-2). *Coatings* **2021**, *11* (4), 388.
(19) Gopal, V.; Nilsson-Payant, B. E.; French, H.; Siegers, J. Y.; Yung, W.-s.; Hardwick, M.; Te Velthuis, A. J. Zinc-Embedded Polyamide Fabrics Inactivate SARS-CoV-2 and Influenza A Virus. *ACS Appl. Mater. Interfaces* **2021**, *13*, 30317.
(20) Aydin Sevinç, B.; Hanley, L. Antibacterial activity of dental composites containing zinc oxide nanoparticles. *J. Biomed. Mater. Res., Part B* **2010**, *94* (1), 22−31.
(21) Seil, J. T.; Webster, T. J. Antibacterial effect of zinc oxide nanoparticles combined with ultrasound. *Nanotechnology* **2012**, *23* (49), 495101.
(22) Antoine, T. E.; Hadigal, S. R.; Yakoub, A. M.; Mishra, Y. K.; Bhattacharya, P.; Haddad, C.; Valyi-Nagy, T.; Adelung, R.; Prabhakar, B. S.; Shukla, D. Intravaginal zinc oxide tetrapod nanoparticles as novel immunoprotective agents against genital herpes. *J. Immunol.* **2016**, *196* (11), 4566−4575.
(23) Ghaffari, H.; Tavakoli, A.; Moradi, A.; Tabarraei, A.; Bokharaei-Salim, F.; Zahmatkeshan, M.; Farahmand, M.; Javanmard, D.; Kiani, S. J.; Esghaei, M.; et al. Inhibition of H1N1 influenza virus infection by zinc oxide nanoparticles: another emerging application of nanomedicine. *J. Biomed. Sci.* **2019**, *26* (1), 1−10.
(24) Applerot, G.; Perkas, N.; Amirian, G.; Girshevitz, O.; Gedanken, A. Coating of glass with ZnO via ultrasonic irradiation and a study of its antibacterial properties. *Appl. Surf. Sci.* **2009**, *256* (3), S3−S8.
(25) Merkl, P.; Long, S.; McInerney, G. M.; Sotiriou, G. A. Antiviral Activity of Silver, Copper Oxide and Zinc Oxide Nanoparticle Coatings against SARS-CoV-2. *Nanomaterials* **2021**, *11* (5), 1312.
(26) Wu, W.; Liu, T.; He, H.; Wu, X.; Cao, X.; Jin, J.; Sun, Q.; Roy, V. A.; Li, R. K. Rhelogical and antibacterial performance of sodium alginate/zinc oxide composite coating for cellulosic paper. *Colloids Surf., B* **2018**, *167*, 538−543.
(27) Rahman, M. M. Polyurethane/Zinc Oxide (PU/ZnO) Composite—Synthesis, Protective Propertyand Application. *Polymers* **2020**, *12* (7), 1535.
(28) Schwartz, V. B.; Thétiot, F.; Ritz, S.; Pütz, S.; Choritz, L.; Lappas, A.; Förch, R.; Landfester, K.; Jonas, U. Antibacterial surface coatings from zinc oxide nanoparticles embedded in poly (n-isopropylacrylamide) hydrogel surface layers. *Adv. Funct. Mater.* **2012**, *22* (11), 2376−2386.
(29) Ghimire, P. P.; Jaroniec, M. Renaissance of Stöber Method for Synthesis of Colloidal Particles: New Developments and Opportunities. *J. Colloid Interface Sci.* **2021**, *584*, 838.
(30) Stöber, W.; Fink, A.; Bohn, E. Controlled Growth of Monodisperse Silica Spheres in The Micron Size Range. *J. Colloid Interface Sci.* **1968**, *26* (1), 62−69.
(31) Mecklenburg, M.; Schuchardt, A.; Mishra, Y. K.; Kaps, S.; Adelung, R.; Lotnyk, A.; Kienle, L.; Schulte, K. Aerographite: ultra lightweight, flexible nanowall, carbon microtube material with outstanding mechanical performance. *Adv. Mater.* **2012**, *24* (26), 3486−3490.
(32) Chatterjee, S.; Murallidharan, J. S.; Agrawal, A.; Bhardwaj, R. Why coronavirus survives longer on impermeable than porous surfaces. *Phys. Fluids* **2021**, *33* (2), 021701.
(33) *FDA Code of Federal Regulations Title 21*. U.S. Food & Drug Administrationhttps://www.accessdata.fda.gov/scripts/cdrh/cfdocs/cfcfr/CFRSearch.cfm?CFRPart=582&showFR=1.
(34) Agarwal, H.; Menon, S.; Kumar, S. V.; Rajeshkumar, S. Mechanistic study on antibacterial action of zinc oxide nanoparticles synthesized using green route. *Chem.-Biol. Interact.* **2018**, *286*, 60−70.
(35) Xie, Y.; He, Y.; Irwin, P. L.; Jin, T.; Shi, X. Antibacterial activity and mechanism of action of zinc oxide nanoparticles against Campylobacter jejuni. *Appl. Environ. Microbiol.* **2011**, *77* (7), 2325−2331.
(36) Raghupathi, K. R.; Koodali, R. T.; Manna, A. C. Size-dependent bacterial growth inhibition and mechanism of antibacterial activity of zinc oxide nanoparticles. *Langmuir* **2011**, *27* (7), 4020−4028.
(37) Sirelkhatim, A.; Mahmud, S.; Seeni, A.; Kaus, N. H. M.; Ann, L. C.; Bakhori, S. K. M.; Hasan, H.; Mohamad, D. Review on zinc oxide nanoparticles: antibacterial activity and toxicity mechanism. *Nano-Micro Lett.* **2015**, *7* (3), 219−242.
(38) Patra, J. K.; Baek, K.-H. Antibacterial activity and synergistic antibacterial potential of biosynthesized silver nanoparticles against foodborne pathogenic bacteria along with its anticandidal and antioxidant effects. *Front. Microbiol.* **2017**, *8*, 167.
(39) Amro, N. A.; Kotra, L. P.; Wadu-Mesthrige, K.; Bulychev, A.; Mobashery, S.; Liu, G.-y. High-resolution atomic force microscopy studies of the Escherichia coli outer membrane: structural basis for permeability. *Langmuir* **2000**, *16* (6), 2789−2796.
(40) Jin, S.-E.; Jin, H.-E. Antimicrobial Activity of Zinc Oxide Nano/Microparticles and Their Combinations against Pathogenic Microorganisms for Biomedical Applications: From Physicochemical Characteristics to Pharmacological Aspects. *Nanomaterials* **2021**, *11* (2), 263.
(41) Ciołek, L.; Biernat, M.; Jaegermann, Z.; Zaczynska, E.; Czarny, A.; Jastrzebska, A.; Olszyna, A. The studies of cytotoxicity and antibacterial activity of composites with ZnO-doped bioglass. *Int. J. Appl. Ceram. Technol.* **2019**, *16* (2), 541−551.
(42) Huang, Y.-W.; Wu, C.-h.; Aronstam, R. S. Toxicity of transition metal oxide nanoparticles: recent insights from in vitro studies. *Materials* **2010**, *3* (10), 4842−4859.
(43) Riddell, S.; Goldie, S.; Hill, A.; Eagles, D.; Drew, T. W. The effect of temperature on persistence of SARS-CoV-2 on common surfaces. *Virol. J.* **2020**, *17* (1), 1−7.
(44) Lin, K.; Marr, L. C. Humidity-dependent decay of viruses, but not bacteria, in aerosols and droplets follows disinfection kinetics. *Environ. Sci. Technol.* **2020**, *54* (2), 1024−1032.

https://doi.org/10.1021/acsbiomaterials.1c01076
ACS Biomater. Sci. Eng. 2021, 7, 5022−5027